Rapid #: -25834376

CROSS REF ID: **361642**

LENDER: **OKT (The University of Tulsa) :: McFarlin Library**

BORROWER: **UMR (Missouri University of Science and Technology) :: Main Library**

TYPE:	Article CC:CCG
JOURNAL TITLE:	Journal of molecular spectroscopy
USER JOURNAL TITLE:	Journal of Molecular Spectroscopy
ARTICLE TITLE:	Rotational spectroscopy and structure of 1,1-dichloro-1-silacyclohex-2-ene
ARTICLE AUTHOR:	Davies, Alexander R.,
VOLUME:	404
ISSUE:	
MONTH:	
YEAR:	2024
PAGES:	111939-
ISSN:	0022-2852
OCLC #:	

Processed by RapidX: 12/18/2025 7:59:30 AM

Journal of Molecular Spectroscopy 404 (2024) 111939

Contents lists available at ScienceDirect

Journal of Molecular Spectroscopy

journal homepage: www.elsevier.com/locate/yjmsp

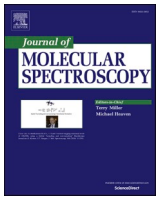

Rotational spectroscopy and structure of 1,1-dichloro-1-silacyclohex-2-ene

Alexander R. Davies [a], Nicole T. Moon [a], Amanda J. Duerden [a], Thomas M.C. McFadden [b], Gamil A. Guirgis [b], Nathan A. Seifert [c], G.S. Grubbs II [a,*]

[a] Department of Chemistry, Missouri University of Science and Technology, 400 W. 11th St., Rolla, MO 65409, USA
[b] Department of Chemistry and Biochemistry, College of Charleston, 66 George St., Charleston, SC 29424, USA
[c] Department of Chemistry and Chemical & Biomedical Engineering, University of New Haven, West Haven, CT 06516, USA

ARTICLE INFO

Keywords:
Chirped-pulse Fourier transform microwave (CP-FTMW) spectroscopy
Isotopologues
Hyperfine splitting
Rotational spectroscopy
Silicon-containing species

ABSTRACT

The ground state rotational spectrum of 1,1-dichloro-1-silacyclohex-2-ene has been recorded using a chirped-pulse Fourier transform microwave (CP-FTMW) spectrometer. Several isotopologues in their natural abundances have been observed in the free-jet expansion, and their spectra assigned, making it possible to present a partial heavy-atom substitution structure. Furthermore, the high resolution of this technique allows the complicated hyperfine splitting pattern to be largely deconvoluted. As a result, the on-diagonal nuclear quadrupole coupling constants for the two chlorine atoms have been determined for all observed isotopologues. Additionally, χ_{bc} is determined for both chlorine atoms of the parent species. The quadrupole coupling tensors for the parent species have been diagonalised, noting some assumptions have been made pertaining to the off-diagonal nuclear quadrupole coupling constants in the principal axis system, to yield reasonable values of χ_{zz} and η which are then compared.

1. Introduction

Very recently [1], we reported the rotational spectra and synthetic methods for 1-silacyclohex-2-ene and 1,1-difluoro-1-silacyclohex-2-ene. The current system, 1,1-dichloro-1-silacyclohex-2-ene, differs from the previous molecules by replacing the two fluorine or hydrogen atoms (bound directly to the silicon atom) with two chlorine atoms. This forms part of an ongoing study into the physicochemical properties of various silicon-containing molecules [1–9]. From this, a number of interesting observations have been made, including ring puckering or twisting motions [4–7], unexpected minimum energy structures [7,8] and, where pertinent, unusual nuclear quadrupole coupling constants (NQCCs) [9]. Herein, we present the results of the microwave spectroscopy of 1,1-dichloro-1-silacyclohex-2-ene.

Chlorinated silicon-containing species have been of interest for many years with the rotational spectrum of chlorosilane [10] having been reported as early as 1948. Since then, we, amongst others, have studied the rotational spectra of various silicon-containing species to determine whether or not there are any chemical, electronic or structural differences between these species and their all-carbon analogues. There are too many rotational studies on chlorinated silanes to reference them individually, however, Refs. [3,9–34] should provide the reader with a flavour of the wealth of information there is about these species. Chlorine-containing molecules are of interest as the presence of the quadrupolar chlorine nucleus ($I = 3/2$) leads to hyperfine splitting, and, if the splitting is adequately resolved and modelled in the constructed Hamiltonian, the determined quadrupole coupling tensor can be used as an indirect probe to understand any changes in the electronic environment immediately surrounding the chlorine nucleus, and therefore the Cl—X (X = C, Si, *etc.*) bonds, between species.

In the case of the titular system, there are two non-equivalent chlorine nuclei bound directly to the silicon atom. The two chlorine nuclei are inequivalent due to the lack of a plane of symmetry in the silacyclohex-2-ene ring system arising from it containing only one carbon–carbon double bond (this is apparent in Fig. 1 when the molecule is viewed in the *ac*-plane). Thus, each chlorine atom has a slightly different "view" of the ring structure and, therefore, the electric fields about the two chlorine nuclei are subtly different. This, then, becomes a somewhat more complicated problem as the numerous resultant hyperfine transitions are often overlapped, typically leading to a spectrum that has broadened activity through unresolved structure and so is more difficult to deconvolute.

* Corresponding author.
E-mail address: grubbsg@mst.edu (G.S. Grubbs).

https://doi.org/10.1016/j.jms.2024.111939
Received 6 June 2024; Received in revised form 12 August 2024; Accepted 27 August 2024
Available online 30 August 2024

2. Experimental and theoretical methods

2.1. Synthesis

This molecule, 1,1-dichloro-1-silacyclohex-2-ene, was synthesised at the College of Charleston and was prepared in the manner described previously [5], but using trichlorosila-5-chloropent-2-ene as an intermediate. It was then purified by trap-to-trap distillation, under vacuum (0.1 Torr), and collected in a trap at −38 °C with a yield of 68 %. The NMR data (^{1}H, ^{13}C and ^{29}Si) are presented in Ref. [1] and the corresponding spectra are given as Supporting Data therein.

2.2. Microwave spectroscopy

The microwave spectrum was recorded at the Missouri University of Science and Technology, in a chirped-pulse Fourier transform microwave (CP-FTMW) spectrometer, that has been described elsewhere [35,36], in the traditional CP-FTMW configuration. The vapour above a highly volatile, liquid sample at room temperature was seeded in 25 psig Ar and passed through the orifice (~760 μm diameter) of a custom-made sample reservoir [37], attached to the exterior of a Parker-Hannifin™ Series 9 solenoid valve (operating at a 3 Hz repetition rate) to form a free-jet expansion. Three separate spectra were obtained in three different regions of the electromagnetic spectrum (5.5–10.25, 9.75–14.75 and 14.0–18.75 GHz), to maintain as high a microwave power as possible, while using a chirped-pulse of 4 μs in temporal width for each region. Three free-induction decays (FIDs), each 20 μs long, were collected per gas pulse and averaged together. Approximately 250,000 FIDs were recorded for each region.

The averaged FIDs were then fast Fourier transformed into the frequency domain, using Kisiel's FFTS software [38,39] with a Bartlett windowing function. Typical linewidths of ~60–80 kHz full-width at half-maximum (FWHM) were achieved, in the absence of other broadening, such as unresolved (hyperfine) splitting. Fits for the various isotopologues were conducted using Pickett's SPCAT/SPFIT [40] programs to a Watson S-reduced Hamiltonian in the I^r representation, with an attributed uncertainty of 10 kHz in the line centres; Kisiel's AABS program [39,41] was used as a user interface for SPCAT/SPFIT. The coupling scheme employed for the two chlorine nuclei was $\boldsymbol{F}_1 = \boldsymbol{J} + \boldsymbol{I}_1$ then $\boldsymbol{F}_{tot} = \boldsymbol{F}_1 + \boldsymbol{I}_2$, where $\boldsymbol{I}_1$ pertains to Cl(A) and $\boldsymbol{I}_2$ to Cl(B) — see Fig. 1. Complete line lists, for all isotopologues, are made available as Supporting Data.

2.3. Computational quantum chemistry

Owing to the anticipated complicated hyperfine splitting, it was imperative to obtain a good prediction of the NQCCs as a starting point for the fit. To do this, the geometry of 1,1-dichloro-1-silacyclohex-2-ene was optimised using the MP2 method, with the aug-cc-pVTZ basis set, to the "tight" convergence criteria as implemented in the Gaussian 16 suite of computational quantum chemistry programs [42] (revision C.01). The nature of the optimised stationary point on the potential energy surface was verified by performing, subsequently, a harmonic frequency calculation and noting the absence of any imaginary frequencies. The "checkpoint" file, as output by Gaussian 16, was used to transform the principal axes and recalculate the rotational constants and NQCCs upon modifying the isotopic masses for the various isotopologues. In addition, natural population analysis (NPA) calculations are also performed utilising the NBO (version 3.1) program [43], as implemented in Gaussian 16. The aforementioned geometry was used, but the density was calculated using the QCISD method with the same basis set which was an attempt to capture as much of the dynamic correlation from the valence electrons as reasonably possible (a total of 20 core orbitals are "frozen" *i.e.*, uncorrelated). Further calculations were conducted on chlorosilane and dichlorosilane, in the manner detailed above, to obtain comparable NPA charges but 10 and 15 core orbitals were frozen, respectively, in the single-point QCISD calculations.

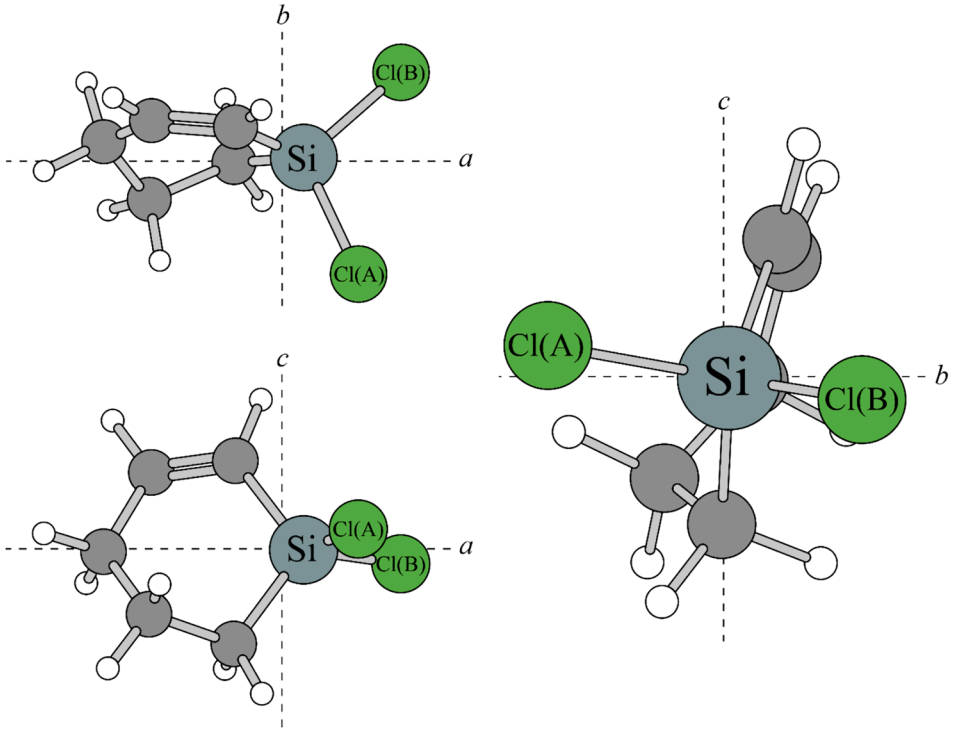

Fig. 1. A view of 1,1-dichloro-1-silacyclohex-2-ene (as calculated by MP2/aug-cc-pVTZ) in the planes defined by the principal axes. The bonds have been drawn in such a way to offer some perspective as to what is pointing into and out of the plane of the paper. Carbon atoms are coloured in grey, hydrogen atoms are white, the silicon atom is teal, and chlorine atoms are in green. The chlorine atoms have been labelled consistently throughout. (For interpretation of the references to colour in this figure legend, the reader is referred to the web version of this article.)

3. Results and discussion

3.1. General commentary

As expected from the calculated dipole moments presented in Table 1, the rotational spectrum is dominated by intense *a*-type transitions belonging to the R-branch, which are split into multiple hyperfine components arising from the various combinations of the allowed changes in the *F* quantum numbers for the two quadrupolar nuclei — the rotational spectrum between 5500 and 18750 MHz is presented in Fig. 2. Only three Q-branch transitions are observed weakly for the parent species, and these were also *a*-type transitions. The hyperfine splitting is generally complicated, and many individual components are unresolved, even with the resolution achieved with our spectrometer. This meant that a significant portion of the hyperfine transitions had to be fit to the same band as part of a "blend". Full details of the lines treated in this manner are given in the Supporting Data. Conversely, particularly for the parent species, some regions of spectral activity are well resolved by the spectrometer detailed in Section 2.2 and an example of this is the $5_{3,2}\ F_1'\ F_{tot}' \leftarrow 4_{3,1}\ F_1''\ F_{tot}''$ transition, depicted in Fig. 3. Therein, the predicted spectrum is presented below, inverted, showing that the experimentally determined spectroscopic parameter values in Table 2 (particularly the NQCCs) reproduce well the experimental spectrum. While this spectrum is overwhelmingly *a*-type, splitting arising from two *b*-type R-branch transitions and one *c*-type R-branch transition is observed weakly for the parent species only — these are the $6_{1,6}\ F_1'\ F_2' \leftarrow 5_{0,5}\ F_1''\ F_{tot}''$, $5_{3,3}\ F_1'\ F_{tot}' \leftarrow 4_{2,2}\ F_1''\ F_{tot}''$ and $5_{3,2}\ F_1'\ F_{tot}' \leftarrow 4_{2,2}\ F_1''\ F_{tot}''$ transitions, centred at approximately 10041, 12,306 and 12344 MHz, respectively.

Further owing to the two non-equivalent quadrupolar nuclei, the complicated hyperfine structure is immediately obvious in the spectrum. In Table 2, there are two sets of data for the parent species: one where the undetermined off-diagonal quadrupole coupling constants are not included in the Hamiltonian (Fit A), and one where those NQCCs are held to their calculated values (Fit B). The advantage to the former approach is that there is no assumed value included in the Hamiltonian and therefore no parameter can be remotely dependent on an undeterminable parameter. Thus, it is expected that the determined constants in Fit A would have more physical meaning than those in Fit B. The advantage to the latter approach is that it is possible to diagonalise the quadrupole coupling tensor in the principal axis system (PAS) into a space-fixed axis system, centred at the quadrupolar nucleus yielding physically meaningful results. Therefore, it is possible to gain a qualitative understanding of the electric field gradient at the chlorine nuclei and to make inferences about the natures of the Si—Cl bonds, and how they compare to one another and to other systems (see Section 2.3 for detailed analysis of the quadrupole coupling tensor). The major disadvantage is that this is approximate, and it is impossible to know for certain whether the calculated values of the off-diagonal NQCCs are reasonable or not — this renders the entire quadrupole coupling tensor semi-experimental. However, given the very good agreement between the experimentally determined NQCCs in Table 2 to those calculated by MP2/aug-cc-pVTZ in Table 1, there is no *prima facie* reason to believe that there would be any significant differences between the calculated off-diagonal NQCCs and those that would be determined experimentally, had this been possible. Finally, further evidence this assumption is not detrimental to the fit is that the values of all determined spectroscopic constants are very close to one another between Fits A and B, and the determined parameter values are largely within the uncertainties of one another, suggesting that these fits are nearly the same to within experimental error.

As implied in the above, the rotational spectra of a few of isotopically substituted species are observed in their natural abundances. The minor isotopologues are referred to by the substituted isotope and, for the chlorine ones, an alphabetical index label (as in Fig. 1) to distinguish between them. The rotational spectra of the following isotopologues are observed: ^{37}Cl(A), ^{37}Cl(B), ^{37}Cl(A)—^{37}Cl(B), ^{29}Si and ^{30}Si. The signal-to-noise was not sufficient to observe any isotopologues arising from ^{13}C substitutions — this is despite a predicted *a*-dipole-moment in excess of 3 D (Table 1). This precludes the determination of a complete heavy-atom substitution structure for this molecule, but it was possible to determine and evaluate some geometric parameters pertaining to the silicon and chlorine atoms, which are presented and discussed in Section 3.4.

While the signal-to-noise was sufficient to observe the doubly substituted ^{37}Cl(A)—^{37}Cl(B) isotopologue and the singly substituted ^{29}Si and ^{30}Si isotopologues (whose natural abundances are approximately 6 %, 5 % and 3 %, respectively, with respect to the major isotope), the transitions arising from these were typically weak. An example of transitions arising from both silicon isotopologues is presented in Fig. 4 and these are amongst the more well-resolved and intense transitions observed. This highlights that there are ample data against which to judge the fit rotational, centrifugal distortion and nuclear quadrupole coupling constants presented in Table 2. Fig. 4 also shows the similarity between the hyperfine structure from the silicon isotopologues and that of the parent species.

3.2. Rotational and centrifugal distortion constants

Comparing the equilibrium rotational constants as calculated by MP2/aug-cc-pVTZ (Table 1) and the experimentally determined rotational constants for the parent species in its ground vibrational state (Table 2), one can see that there is very good agreement between the pairs of values. Indeed, the calculated rotational constants are within 1

Table 1
Spectroscopic parameters, and their values, for all observed isotopologues of 1,1-dichloro-1-silacyclohex-2-ene, as calculated by MP2/aug-cc-pVTZ.

	Parent	^{37}Cl(A)	^{37}Cl(B)	^{37}Cl(A)—^{37}Cl(B)	^{29}Si	^{30}Si
A_e/MHz	1616.5823	1584.0799	1596.5916	1563.3381	1616.5631	1616.5442
B_e/MHz	925.8255	920.4986	913.7231	909.0374	925.6256	925.4286
C_e/MHz	790.3679	779.1467	777.0754	766.1975	790.2182	790.0707
Cl(A) χ_{aa}/MHz	8.7094	6.2906	9.5449	6.9948	8.7128	8.7161
Cl(A) $\chi_{bb} - \chi_{cc}$/MHz	−41.2871	−32.2274	−42.2688	−33.0305	−41.2906	−41.2939
Cl(A) χ_{ab}/MHz	18.7819	15.3310	18.0200	14.7321	18.7789	18.7759
Cl(A) χ_{ac}/MHz	−3.7291	−2.8576	−3.4719	−2.6634	−3.7284	−3.7278
Cl(A) χ_{bc}/MHz	7.0515	5.1121	6.9044	5.0094	7.0517	7.0520
Cl(B) χ_{aa}/MHz	−10.9704	−9.9853	−9.5682	−8.8265	−10.9750	−10.9796
Cl(B) $\chi_{bb} - \chi_{cc}$/MHz	−22.4245	−23.5454	−16.8639	−17.7017	−22.4204	−22.4162
Cl(B) χ_{ab}/MHz	−25.9319	−26.0466	−20.3551	−20.4743	−25.9315	−25.9312
Cl(B) χ_{ac}/MHz	4.2153	3.9169	3.1966	2.9738	4.2149	4.2145
Cl(B) χ_{bc}/MHz	3.9610	3.8412	2.8828	2.7951	3.9599	3.9589
$\lvert\mu_a\rvert$/D	3.1210	3.1302	3.1085	3.1187	3.1209	3.1209
$\lvert\mu_b\rvert$/D	0.4784	0.4244	0.5500	0.4985	0.4787	0.4790
$\lvert\mu_c\rvert$/D	0.3799	0.3679	0.3846	0.3726	0.3799	0.3800

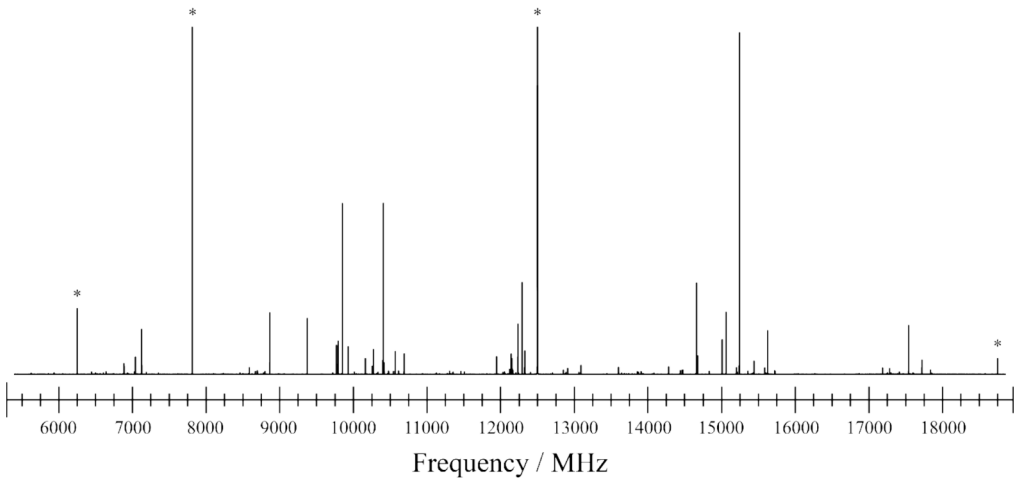

Fig. 2. The rotational spectrum of 1,1-dichloro-1-silacyclohex-2-ene in the 5500–18,750 MHz of the electromagnetic spectrum. The three separate rotational spectra (see Section 2.2) have been spliced together, and the intensities have been scaled such that the noise floors of each region are approximately of the same intensity. The peaks marked with an asterisk ("*") are artificial, corresponding to an internal clock frequency of the oscilloscope (12,500 MHz), and the most intense harmonics of this (6250, 7812.5 and 18,750 MHz).

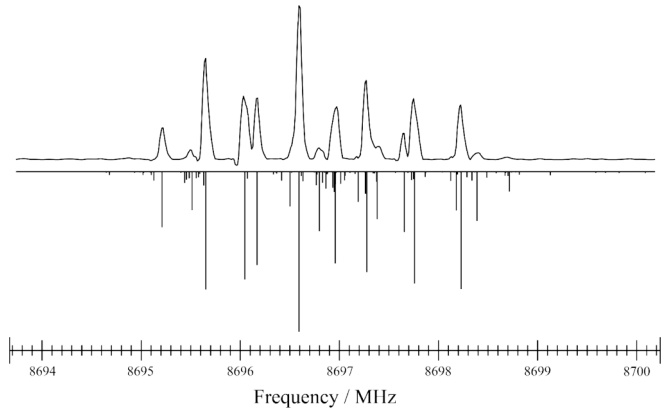

Fig. 3. An example of one of the more well-resolved features in the rotational spectrum of the parent species of 1,1-dichloro-1-silacyclohex-2-ene, between 8694 and 8700 MHz, showing well-resolved hyperfine splitting arising from the two non-equivalent chlorine atoms. The depicted transition is the $5_{3,2}$ F_1' $F'_{tot} \leftarrow$ $4_{3,1}$ F_1'' F''_{tot} transition, and the predicted spectrum is shown inverted.

% of the experimental values, indicating that this inexpensive method (for molecules of this size) with a modest basis set, yields a sufficiently accurate structure as a starting point for investigating the experimental rotational spectrum. As the rotational constants for the minor isotopologues are calculated from the geometry and electronic structure of the parent species, and only the mass of the appropriate atoms is changed, it is unsurprising (although reassuring) that there is also good agreement between the experimentally determined and calculated rotational constants for all isotopologues in Tables 1 and 2.

For the parent species only, it was possible to determine all five quartic centrifugal distortion constants. It was not possible to determine uniquely D_K and d_2 for any minor isotopologue, nor was it possible to determine d_1 for the ^{37}Cl(A)—^{37}Cl(B), ^{29}Si or ^{30}Si species — the value of D_{JK} was also not determinable for the ^{30}Si isotopologue. In all cases where a centrifugal distortion constant for a minor isotopologue was not determinable, it was held to the corresponding value for the parent species as found in Fit A (see Table 2). However, one can see that while there is some variation in the rotational and centrifugal distortion constants between Fits A and B (Table 2), this difference is very small and the rotational constants and centrifugal distortion constants are within error of one another. Consequently, it is acknowledged that the effect on the quality of the fits for the minor isotopologues would be minimal whether the centrifugal distortion constants are held to those in Fit A or Fit B.

When considering the number of transitions, the rotational constants and centrifugal distortion constants are determined based on the locations of the transitions in absence of hyperfine splitting. For this reason, in Table 2, the number of transitions that comprise the fit are provided alongside the number of unique frequency lines (*i.e.*, including all transitions that form part of a blend as a single line) and the number of transitions when one discounts hyperfine splitting. For example, only 10 transitions with different J, K_a and K_c quantum numbers are observed for the ^{30}Si isotopologue.

3.3. Nuclear quadrupole coupling

Firstly, we address the largest discrepancies between Fits A and B, which are the values of χ_{aa} and χ_{bb}-χ_{cc} for Cl(B), where the former is −10.7113(87) MHz in Fit A and −10.7007(87) MHz in Fit B, and the latter is −24.352(22) MHz in Fit A and −24.378(22) MHz in Fit B. In both cases, there is still significant overlap of the uncertainties. This would lead one to conclude that the approximate, semi-experimental quadrupole coupling tensors in the PAS are likely very good approximations of the "true" quadrupole coupling tensors (at least to within the experimental data available) and, therefore, any conclusions made from the diagonalised quadrupole coupling tensor can be viewed, at the very least, as qualitatively correct.

It is not possible to determine the signs of the individual off-diagonal NQCCs from a microwave experiment, merely their magnitudes and the sign-product of all three off-diagonal NQCCs [44]. As such, in Table 2, only the absolute values of the off-diagonal NQCCs are given. However, for transparency, a negative sign for both χ_{bc} parameters was used for Fit A (see the Supporting Data) in order to be consistent with the calculated sign-products of the off-diagonal components of both quadrupole coupling tensors. The predicted signs of the off-diagonal quadrupole coupling constants are given, for reference, in Table 1. Needless to say, the chosen signs of the off-diagonal quadrupole coupling constants in Fit B correlate exactly to those predicted by the quantum chemical calculation.

The calculated and semi-experimental quadrupole coupling tensors for the parent species have been diagonalised using Kisiel's QDIAG program, which is available on the PROSPE website [39] (output files are provided as Supporting Data). The values of χ_{zz}, $|\eta|$ and θ_{za} for both atoms are presented in Table 3. These parameters are, respectively: the

Table 2
Experimentally determined spectroscopic parameters, and their values, for the observed isotopologues of 1,1-dichloro-1-silacyclohex-2-ene[a].

	Parent[b]		^{37}Cl(A)	^{37}Cl(B)	^{37}Cl(A)—^{37}Cl(B)	^{29}Si	^{30}Si
	Fit A	Fit B					
A_0/MHz	1626.78267(91)	1626.78211(88)	1594.6339(29)	1606.3925(31)	1573.5000(33)	1626.7826(67)	1626.799(17)
B_0/MHz	928.28530(20)	928.28517(19)	922.81721(28)	916.47176(29)	911.64396(34)	928.09623(49)	927.90537(85)
C_0/MHz	796.47063(18)	796.47067(17)	785.13052(25)	783.18134(26)	772.18396(22)	796.32926(62)	796.19049(70)
D_J/MHz	$3.212(63) \times 10^{-5}$	$3.199(60) \times 10^{-5}$	$2.920(87) \times 10^{-5}$	$3.304(89) \times 10^{-5}$	$2.79(13) \times 10^{-5}$	$3.04(40) \times 10^{-5}$	$2.36(36) \times 10^{-5}$
D_K/MHz	$-1.73(33) \times 10^{-4}$	$-1.85(31) \times 10^{-4}$	$[-1.73 \times 10^{-4}]$	$[-1.73 \times 10^{-4}]$	$[-1.73 \times 10^{-4}]$	$[-1.73 \times 10^{-4}]$	$[-1.73 \times 10^{-4}]$
D_{JK}/MHz	$4.454(41) \times 10^{-4}$	$4.442(39) \times 10^{-4}$	$4.76(10) \times 10^{-4}$	$4.675(75) \times 10^{-4}$	$4.69(27) \times 10^{-4}$	$4.91(35) \times 10^{-4}$	$[4.454 \times 10^{-4}]$
d_1/MHz	$-1.142(68) \times 10^{-5}$	$-1.127(65) \times 10^{-5}$	$-1.091(77) \times 10^{-5}$	$-7.79(86) \times 10^{-6}$	$[-1.142 \times 10^{-5}]$	$[-1.142 \times 10^{-5}]$	$[-1.142 \times 10^{-5}]$
d_2/MHz	$-3.40(40) \times 10^{-6}$	$-3.26(38) \times 10^{-6}$	$[-3.40 \times 10^{-6}]$	$[-3.40 \times 10^{-6}]$	$[-3.40 \times 10^{-6}]$	$[-3.40 \times 10^{-6}]$	$[-3.40 \times 10^{-6}]$
Cl(A) χ_{aa}/MHz	8.7293(80)	8.7280(73)	6.183(23)	9.601(19)	7.057(45)	8.63(10)	8.29(24)
Cl(A) $\chi_{bb}-\chi_{cc}$/MHz	−43.220(19)	−43.218(18)	−33.876(56)	−44.092(52)	−34.312(88)	−43.67(19)	−43.00(40)
Cl(A) $\lvert\chi_{ab}\rvert$/MHz	–	[18.781878]	–	–	–	–	–
Cl(A) $\lvert\chi_{ac}\rvert$/MHz	–	[3.729118]	–	–	–	–	–
Cl(A) $\lvert\chi_{bc}\rvert$/MHz	6.87(24)	6.78(23)	–	–	–	–	–
Cl(B) χ_{aa}/MHz	−10.7113(87)	−10.7007(87)	−9.716(21)	−9.382(17)	−8.757(53)	−10.893(80)	−10.38(25)
Cl(B) $\chi_{bb}-\chi_{cc}$/MHz	−24.352(22)	−24.378(22)	−25.564(68)	−18.624(48)	−19.368(96)	−25.10(19)	−24.40(48)
Cl(B) $\lvert\chi_{ab}\rvert$/MHz	–	[25.931866]	–	–	–	–	–
Cl(B) $\lvert\chi_{ac}\rvert$/MHz	–	[4.2152757]	–	–	–	–	–
Cl(B) $\lvert\chi_{bc}\rvert$/MHz	4.32(25)	4.37(24)	–	–	–	–	–
N[c]	680 {536} ⟨77⟩	680 {536} ⟨77⟩	382 {254} ⟨52⟩	381 {261} ⟨49⟩	156 {99} ⟨26⟩	74 {54} ⟨16⟩	47 {26} ⟨10⟩
MW RMS[d]/kHz	9.9	9.5	9.2	8.6	8.1	9.4	8.9

[a] Numbers in brackets give the standard errors (67% confidence interval), pertaining to the least significant figures. Numbers in square brackets have been held to the parent, or calculated, value — see text for details.

[b] Two fits for the parent species are provided: one where χ_{ab} and χ_{ac} are excluded from the Hamiltonian (Fit A) and one where these are held to their calculated value (Fit B) — see text for details.

[c] Number of transitions included in the fit. This is inclusive of all hyperfine components belonging to each rotational transition. The number of unique frequency lines is given in curly brackets and the number of unique J, K_a, K_c states are given in angle brackets.

[d] MW RMS is defined as: $\sqrt{\frac{\sum_i (o_i - c_i)^2}{N}}$, where o_i is the observed frequency of the i^{th} transition, c_i is its calculated frequency, and N is the number of transitions included in the fit.

quadrupole coupling constant along the z-axis, a measure of the asymmetry of the electric field gradient along the z-axis and the angle of rotation between the space-fixed z-axis and the principal a-axis. For the purposes of diagonalising the quadrupole coupling tensor, it is assumed the resultant z-axis is coincident with, or very close to, the Si—Cl bond. The value of η is defined as $\frac{\chi_{xx}-\chi_{yy}}{\chi_{zz}}$ and is often given as an absolute value because, once the z-axis is defined, the choice of which of the orthogonal axes is x and which is y is arbitrary; this choice does not affect the value or sign of χ_{zz} or θ_{za}. For full and technical details of the transformation to the space-fixed coordinate system, please see the Supporting Data.

As it was necessary to hold the values of χ_{ab} and χ_{ac} to the calculated values (Fit B) to yield meaningful results, the uncertainties on these parameter values were taken to be zero, hence the uncertainties on the values of χ_{zz}, $|\eta|$ and θ_{za} are somewhat lower than one might expect had it been possible to determine all three off-diagonal NQCCs explicitly. No attempt is made to diagonalise the quadrupole coupling tensors for the minor isotopologues as no off-diagonal quadrupole coupling constants were determinable for any of these. Therefore, half of the components in the quadrupole coupling tensor would be assumed from calculation (noting that χ_{bb} and χ_{cc} can be individually determined from χ_{aa} and χ_{bb}-χ_{cc}, as the quadrupole coupling tensor is traceless). Given the arguments below are already rendered qualitative for the parent species, it is not believed that any useful information would come out of this process. It may be possible to compare the values of χ_{zz} to that of the parent species but given the number of assumptions made of the quadrupole coupling tensors in the PAS, it would be difficult to say whether any deviations or similarities to the expected quadrupole moment ratio, 1.26889(3) [45], are genuine or constructed.

The data presented in Table 3 show that the MP2/aug-cc-pVTZ method has calculated the electric fields about the two quadrupolar nuclei reasonably when compared to the experimental data. However, it is acknowledged that the use of the data from Fit B does include parameter values held to the calculated values, which will somewhat influence the determined values of χ_{zz}, θ_{za} and $|\eta|$. Notably, the value of χ_{zz} for Cl(B) is slightly more negative, even when one considers the uncertainty on these values, suggesting that the two chlorine nuclei are (subtly) inequivalent.

Nonetheless, the values of χ_{zz} are about −35 MHz and $|\eta|$ is about zero (highly cylindrically symmetric electronic distribution about the bonds). This is consistent with other species, chiefly chlorosilane (χ_{zz} = −39.6956(23) MHz [23]) and dichlorosilane (χ_{zz} = −38.33(13) MHz [24]), although the values of χ_{zz} are notably more negative in the case of these two small silanes. If one employs a Townes-Daily analysis [46,47] (see also Refs. [48,49]), one can, to a reasonable degree of accuracy, estimate the ionic character of a bond from a measurement of χ_{zz} (recalling $\chi_{zz} = eQq_{zz}$, where Q is the quadrupole moment of the nucleus, e is the charge of the electron and q_{zz} is the electric field gradient along the z-axis). This typically assumes that only the valence p electrons make a significant contribution to the electric field gradient, q_{zz}, at the quadrupolar nucleus. (It is also assumed that the halogen is the negative pole of the bond, and this is reasonable if one consults the NPA charges in Table 4.) Consequently, it can be interpreted that the further away χ_{zz} gets from the idealised quadrupole coupling constant from a single $3p_z$ electron orbiting a free chlorine atom ($-eQq_{3,1,0}$ = −109.74 MHz [49]) towards a value of zero, the more ionic the bond is — although differences in orbital hybridisation may also have an effect if there is significantly different hybridisation between the species, which is neglected here. Thus, it is possible to arrive at the conclusion that the two Si—Cl bonds in 1,1-dichloro-1-silacyclohex-2-ene are more ionic than those in chlorosilane and dichlorosilane, and that the Si—Cl(A) bond is more ionic than that of Si—Cl(B).

This is consistent with the NPA charges in Table 4: while the chlorine atoms have approximately the same charge in all species (∼−0.40 e), the silicon atom in 1,1-dichloro-1-silacyclohex-2-ene is notably more electropositive (at a significant +1.59 e) than it is in dichlorosilane (+1.16 e)

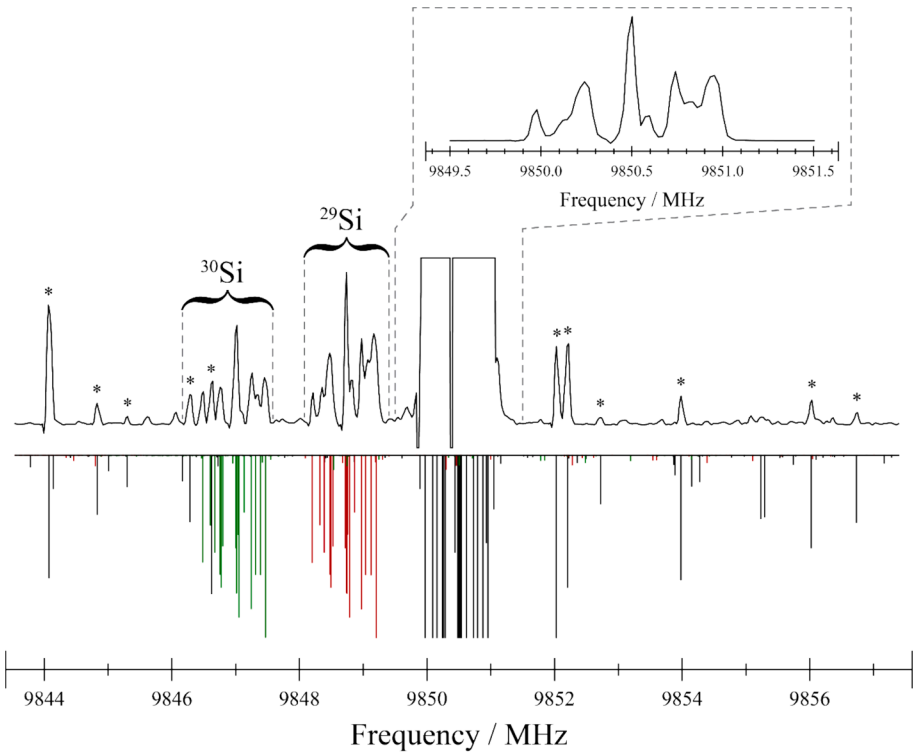

Fig. 4. A portion of the rotational spectrum of the parent species of 1,1-dichloro-1-silacyclohex-2-ene, between approximately 9844 and 9857 MHz, showing an example of a transition of the parent species alongside the corresponding transitions for the ^{30}Si and ^{29}Si isotopologues, which are moderately intense and well-resolved. The depicted transition is the $6_{1,6}$ F_1' F_{tot}'←$5_{1,5}$ F_1'' F_{tot}'' transition for all species. The feature pertaining to the ^{30}Si isotopologue is overlapped by some weaker transitions arising from the parent species, which are marked with an asterisk ("*") on the zoomed-in portion of the spectrum. Shown inverted are the spectra predicted from the spectroscopic constants in Table 2 for the parent species (black), ^{29}Si isotopologue (red) and the ^{30}Si isotopologue (green). The predicted spectrum for the parent species has been enlarged to show the transitions overlapping the ^{30}Si isotopologue feature and the most intense transitions (black and centre) have been truncated. The relative intensity scales for the predicted spectra of the isotopologues are not to scale and have been normalised to an arbitrary maximum. (For interpretation of the references to colour in this figure legend, the reader is referred to the web version of this article.)

Table 3
Results of diagonalising the nuclear quadrupole coupling tensor in the principal axis system (PAS) into a space-fixed axis system.[a,b]

		MP2/aug-cc-pVTZ	Parent (Fit B)
Cl(A)	χ_{zz}[c]/MHz	−34.6239	−35.322(61)
	$\lvert\eta\rvert$[d]	0.0329	0.0563(21)
	θ_{za}[e]/°	113.8327	113.480(26)
Cl(B)	χ_{zz}[c]/MHz	−35.0590	−35.467(38)
	$\lvert\eta\rvert$[d]	0.0123	0.0338(46)
	θ_{za}[e]/°	42.5175	43.310(44)

[a] Diagonalisation of the quadrupole coupling tensor in the PAS requires a complete tensor to yield meaningful results. The values of χ_{ab} and χ_{ac} were held to the calculated values — see text and Table 2 for further details and discussion.
[b] The value of χ_{zz} for chlorosilane is −39.6956(23) [23], and −38.33(13) for dichlorosilane [24].
[c] The z-axis is assumed to lie along, or very close to, the Cl—Si bond.
[d] This is a measure of the asymmetry of the electric field gradient along the z-axis: $\eta = \frac{\chi_{xx} - \chi_{yy}}{\chi_{zz}}$. A value of zero represents perfect cylindrical symmetry.
[e] This is the angle of rotation between the space-fixed z-axis and the principal a-axis.

which, in turn, has a more electropositive silicon atom than chlorosilane (+1.00 e). Therefore, the increasing value of χ_{zz} (less negative) from chlorosilane to the titular molecule is commensurate with an increasing difference in the charges on the silicon and chlorine atoms and therefore increasing ionic character of the bond. The difference in charges between Si and Cl(A) in 1,1-dichloro-1-silacyclohex-2-ene is greater than that between Si and Cl(B) and this is also consistent with the value of χ_{zz} for Cl(A) being the closest to zero of the pair, and therefore having the more ionic bond to the silicon atom (compare Tables 3 and 4). This difference in the calculated charges is quite subtle, and this is reflected in the very small differences in the values of χ_{zz} for the two chlorine nuclei, although it is reiterated that the two values of χ_{zz} are not within the uncertainty of one another, and we are therefore satisfied that these values are meaningfully different. This effect is more pronounced when one compares the values of χ_{zz} and the NPA charges of 1,1-dichloro-1-silacyclohex-2-ene with those of dichlorosilane and chlorosilane: chlorosilane has the smallest difference between the charges on the silicon and chlorine atoms and has the most negative value of χ_{zz}. From this, we can conclude that the electronic environments about Cl(A) and Cl(B) are very similar, but measurably different.

Table 4
Calculated NPA charges (q) on the silicon and chlorine atoms for chlorosilane, dichlorosilane and 1,1-dichloro-1-silacyclohex-2-ene.

	q_{Si}	q_{Cl}	$q_{Si} - q_{Cl}$
Chlorosilane (SiH_3Cl)	0.9979	−0.3968	1.3947
Dichlorosilane (SiH_2Cl_2)	1.1632	−0.3773	1.5405
1,1-dichloro-1-silacyclohex-2-ene — Cl(A)	1.5914	−0.3767	1.9681
1,1-dichloro-1-silacyclohex-2-ene — Cl(B)		−0.3677	1.9591

3.4. Experimental substitution (r_s) structure

Having observed the rotational spectra of species for numerous isotopologues of 1,1-dichloro-1-silacyclohex-2-ene, it is possible to determine a partial substitution (r_s) structure for the molecule. As the signal-

to-noise was not good enough to observe isotopologues due to ^{13}C substitution, it is only possible to determine the Cl(A)—Si and Cl(B)—Si bond lengths, and the Cl(A)—Si—Cl(B) bond angle. This, alongside the low natural abundance of ^{2}H and the monoisotopic nature of fluorine, means it is not possible to draw any direct experimental structural comparisons between the titular system and the highly related systems in Ref. [1]. The bond lengths and angles for 1,1-dichloro-1-silacyclohex-2-ene are presented in Table 5, alongside the corresponding values pertaining to the equilibrium structure (r_e) as calculated by MP2/aug-cc-pVTZ. The experimentally determined and calculated atomic coordinates in the PAS are presented in Table 6.

The positions of the atoms are calculated using Kraitchman's equations [50], using Kisiel's KRA program (as available on the PROSPE website [39] and the output is provided as Supporting Data). As it is the rotational constants of the pertinent isotopologues and the differences in mass with respect to the parent species that are required to calculate the atomic coordinates, only the errors in the rotational constants are propagated into the errors in the resultant coordinates — and these are given according to the criteria of Costain [51]. This process cannot obtain the signs of the coordinates, only their magnitudes; therefore, the signs of the coordinates are assumed from the MP2 r_e structure. In addition, when an atom is very close to a principal axis, Kraitchman's equations may fail to calculate a real coordinate and may also present a large error in that position [50–53] — this is the case here with the *c*-coordinate of the silicon atom (Fig. 1) regardless of whether one uses the rotational constants and mass difference pertaining to substitution of ^{29}Si or ^{30}Si; with the latter substitution, the *b*-coordinate becomes imaginary as well (Table 6). In these instances, the coordinate is assumed to be zero, however the (large) uncertainty in that coordinate is retained. Once the atomic coordinates have been established, it is then possible to evaluate the various geometric parameter values, such as bond lengths and angles (Table 5) — to do this, Kisiel's EVAL program is used (also available on the PROSPE website [39] and the output is provided as Supporting Data). The rotational constants of Fit A for the parent species were used, to be consistent with the methodology used for the fits of the minor isotopologues.

Firstly, both the geometric parameter values in Table 5 and the atomic coordinates in Table 6 are, in general, in good agreement with the corresponding theoretical r_e values. Typically, r_e and r_s (and indeed also r_0) structures are not directly comparable as they are probing a different point on the potential energy surface; however, the two sets of data can be compared insofar as to give an idea of whether the experimentally determined structure is reasonable. That the two structures are in agreement gives reassurance that the fits for the various isotopologues are themselves reasonable.

In Tables 5 and 6, datasets for substitution of ^{28}Si with both ^{29}Si and ^{30}Si are provided as both the ^{29}Si and ^{30}Si isotopologues were observed. One can typically assume that isotopic substitution does not significantly change the geometry of the molecule and, therefore, one can normally expect the substitution structures utilising the rotational constants of ^{29}Si and ^{30}Si to be the same. In Table 5, one can see that for the parameters containing silicon, the values are noticeably different between the two isotopes. However, it should be emphasised that the values for the ^{29}Si dataset are within the uncertainty of the ^{30}Si dataset, and *vice versa*, and therefore both datasets agree — this is also evident if one considers the determined atomic coordinates of the Si atom in Table 6. There is significant uncertainty associated with the parameter values (from either ^{29}Si or ^{30}Si substitution) and this is for two reasons. Firstly, the silicon atom is close to the principal axes and results in imaginary coordinates and high uncertainties associated with them. Secondly, this is compounded by the few transitions observed for these species (Table 2), meaning there is a significant level of uncertainty in the rotational constants as well. Given the determined rotational constants for the ^{30}Si isotopologue have greater uncertainty than those for the ^{29}Si isotopologue (Table 2), and both the *b*- and *c*-coordinates are assumed to be zero when substituting ^{30}Si, the geometric parameter values when substituting ^{29}Si are viewed to be more reliable and so we shall only consider these henceforth. Indeed, the uncertainties on the ^{29}Si—Cl(A) and ^{29}Si—Cl(B) bond lengths contain the theoretical r_e values.

To provide context for these bond lengths, in Table 7 a series of Si—Cl bond lengths and Cl—Si—Cl bond angles are presented for various, small, silicon-containing molecules. One can see that the derived Si—Cl(A) and Si—Cl(B) bond lengths are similar to all other experimentally determined Si—Cl bonds, when considering the uncertainties in these values, although the Si—Cl(B) bond length is notably longer than that in $SiCl_4$, and slightly longer than that of SiH_2Cl_2. Perhaps the closest molecule, structurally, in Table 7 to 1,1-dichloro-1-silacyclohex-2-ene is $Si(CH_3)_2Cl_2$ as the silicon atom is also bonded to two carbon atoms, although the geometry of that system is not constrained by having those two carbon atoms connected as part of a ring structure. The Si—Cl bond length of $Si(CH_3)_2Cl_2$ is determined to be 2.055(3) Å [32] and this is contained within the uncertainties of both the Si—Cl(A) and Si—Cl(B) suggesting that, to within the data available, having the silicon atom as part of a ring structure is having little impact on the bond lengths that the silicon atom has with the two chlorine atoms.

The Cl—Si—Cl bond angle presented in Table 5 — 106.59(46)° for ^{29}Si substitution — compares very well to the calculated r_e bond angle (106.7986°) and the agreement is within 1°, even when one considers the uncertainty on the experimental value. Further consultation of Table 7 reveals that this experimentally determined bond angle is comparable to other systems in which the central silicon atom adopts a

Table 5
Experimentally determined substitution structure (r_s) parameters, and their values, compared to the corresponding theoretical equilibrium (r_e) values, as calculated by MP2/aug-cc-pVTZ.

	Experimental[a] (r_s)	MP2/aug-cc-pVTZ (r_e)
r[Cl(A)—^{29}Si]/Å	2.030(47)	2.0661
r[Cl(A)—^{30}Si]/Å	2.003(53)	
r[Cl(B)—^{29}Si]/Å	2.071(35)	2.0607
r[Cl(B)—^{30}Si]/Å	2.090(40)	
r[Cl(A)—Cl(B)]/Å	3.2878(19)	3.3130
θ[Cl—^{29}Si—Cl]/°	106.59(46)	106.7986
θ[Cl—^{30}Si—Cl]/°	106.90(47)	

[a] Numbers in brackets are the Costain errors [51] pertaining to the least significant figures.

Table 6
Determinable atomic coordinates (Å) of 1,1-dichloro-1-silacyclohex-2-ene, in the principal axis system, as given by Kraitchman substitution (r_s)[a,b,c], and the corresponding equilibrium (r_e) coordinates, as calculated by MP2/aug-cc-pVTZ.

	a	*b*	*c*
Experimental r_s coordinates			
Cl(A)	1.2294(12)	−1.76823(85)	0.2976(51)
Cl(B)	1.85698(81)	1.4159(11)	−0.2289(66)
^{29}Si	0.3354(46)	0.030(52)	0.000(52)[d]
^{30}Si	0.3374(46)	0.000(59)[d]	0.000(53)[d]
Calculated r_e coordinates			
Cl(A)	1.2113	−1.7867	0.3153
Cl(B)	1.8845	1.4100	−0.2359
Si	0.3441	0.0590	−0.0160

[a] The signs of the experimentally determined coordinates have been assumed from the quantum chemical calculation.
[b] The results of substitution of ^{28}Si with ^{29}Si and ^{30}Si are presented for comparison — see text for discussion.
[c] Numbers in brackets are the Costain errors [51] pertaining to the least significant figures.
[d] Owing to the Si atom lying very close to the *b* and *c* principal axes, some coordinates were found to be imaginary. In these cases, the coordinate was assumed to be zero and the uncertainty was retained.

Table 7
Si—Cl bond lengths and Cl—Si—Cl bond angles for various chlorinated silanes.[a]

Molecule	Parameter	Calculated[b]	Experimental	Reference
SiCl	r[Si—Cl]/Å	2.0802[c]	–	
SiH_3Cl	r[Si—Cl]/Å	2.0665	2.05057(6)	[29]
$SiCl_2$	r[Si—Cl]/Å θ[Cl—Si—Cl]/°	2.0856 100.9400	2.0700(12) 101.25(10)	[30]
SiH_2Cl_2	r[Si—Cl]/Å θ[Cl—Si—Cl]/°	2.0506 109.5531	2.033(3) 109.72(33)	[31]
$Si(CH_3)_2Cl_2$	r[Si—Cl]/Å θ[Cl—Si—Cl]/°	2.0667 107.4852	2.055(3) 107.2(3)	[32]
$SiCl_4$	r[Si—Cl]/Å θ[Cl—Si—Cl]/°	2.0298 109.4712	2.0182(3) 109.33(4)	[54]
1,1-dichloro-1-silacyclohex-2-ene	r[^{29}Si—Cl(A)]/Å r[^{29}Si—Cl(B)]/Å θ[Cl—^{29}Si—Cl]/°	2.0661 2.0607 106.7986	2.030(47) 2.071(35) 106.59(46)	This work

[a] The experimental structural parameters for $SiCl_2$ and SiH_3Cl pertain to r_0 structures, and the experimental structural parameter values for $SiCl_4$ are from gas electron diffraction measurements. The remaining experimental entries in this table all pertain to r_s structures.
[b] Calculated (r_e) values using MP2/aug-cc-pVTZ (this work) — see Section 2.3 for details.
[c] Spin-restricted open-shell MP2.

tetrahedral geometry, namely $SiCl_4$, SiH_2Cl_2 and $Si(CH_3)_2Cl_2$, where the bond angles are 109.33(4)° [54], 109.72(33)° [31] and 107.2(3)° [32], respectively.

4. Conclusions

We have synthesised and recorded and analysed the rotational spectrum of 1,1-dichloro-1-silacyclohex-2-ene using chirped-pulse Fourier transform microwave spectroscopy and report the spectroscopic results for the first time. The rotational constants, quartic centrifugal distortion constants, and both on-diagonal NQCCs and χ_{bc} (for both non-equivalent chlorine atoms) were determined for the parent species. In addition to this, we have observed and assigned the rotational spectra of multiple minor isotopologues, in their natural abundances, including those arising from substitution of ^{35}Cl with ^{37}Cl and also ^{28}Si with ^{29}Si and ^{30}Si. This enabled a partial substitution structure to be presented, which is in agreement with that calculated using the MP2 method with the aug-cc-pVTZ basis set and the experimentally determined structures for other chlorinated silanes. Finally, the quadrupole coupling tensor for the parent species was diagonalised, noting that the values of χ_{ab} and χ_{ac} had to be assumed to be the calculated values (the determined NQCCs in the PAS are in good agreement with those calculated), and the resultant values of χ_{zz} for both chlorine nuclei are consistent with those calculated and those of chlorosilane and dichlorosilane. The values of χ_{zz} were also rationalised in terms of the calculated charges on the silicon and chlorine atoms, and by interpreting these values using the theory laid out by Townes and Dailey [46,47], from which we conclude that the Si—Cl(A) bond is subtly more ionic than that of Si—Cl(B) and both are more ionic than those of the Si—Cl bonds in chlorosilane and dichlorosilane. It is also established that electronic environments about the two chlorine atoms are very similar; however, through analysis of the quadrupole coupling tensor, these electronic environments are measurably different.

CRediT authorship contribution statement

Alexander R. Davies: Writing – review & editing, Writing – original draft, Visualization, Validation, Investigation, Formal analysis, Data curation. **Nicole T. Moon:** . **Amanda J. Duerden:** Writing – review & editing, Validation, Investigation, Formal analysis, Data curation. **Thomas M.C. McFadden:** Writing – review & editing, Validation, Investigation, Formal analysis, Data curation. **Gamil A. Guirgis:** Writing – review & editing, Validation, Supervision, Resources, Project administration, Methodology, Investigation, Funding acquisition, Formal analysis, Data curation, Conceptualization. **Nathan A. Seifert:** Writing – review & editing, Validation, Investigation, Formal analysis, Data curation. **G.S. Grubbs:** .

Declaration of competing interest

The authors declare the following financial interests/personal relationships which may be considered as potential competing interests: Garry Grubbs II reports financial support was provided by National Science Foundation. I am a guest editor of the Student Research VSI and have been on the editorial board of J. Mol. Spectrosc. Previously. GSG2 If there are other authors, they declare that they have no known competing financial interests or personal relationships that could have appeared to influence the work reported in this paper.

Data availability

The data that support the findings of this work are contained within the article and the corresponding Supporting Data.

Acknowledgements

This material is based upon work supported by the National Science Foundation under Grant No. CHE-MRI-2019072. A.R.D., N.T.M, A.J.D and G.S.G. II are also grateful for access to the high-performance computing facility, The Foundry, at the Missouri University of Science and Technology, which is supported by the National Science Foundation under Grant No. OAC-1919789.

Appendix A. Supplementary material

Results of the diagonalisation of the quadrupole coupling tensor (experimental and calculated) and Kraitchman substitution, as well as complete line lists and technical details of the fits (all isotopologues) are given as Supporting Data. Supplementary data to this article can be found online at https://doi.org/10.1016/j.jms.2024.111939.

References

[1] N.T. Moon, A.J. Duerden, T.M.C. McFadden, N.A. Seifert, G.A. Guirgis, G. S. Grubbs II, Rotational spectrum and ring structures of silacyclohex-2-ene and 1,1-difluorosilacyclohex-2-ene, J. Phys. Chem. A 128 (2024) 10–19, https://doi.org/10.1021/acs.jpca.3c04027.
[2] J.R. Glenn, J.E. Isert, J.D. Bethke, G.A. Guirgis, G.S. Grubbs II, The microwave spectrum of the low energy conformers of 1-ethylsilacyclopentane, J. Mol. Spectrosc. 399 (2024) 111872, https://doi.org/10.1016/j.jms.2023.111872.
[3] T. Pulliam, F.E. Marshall, T. Carrigan-Broda, D.V. Hickman, G. Guirgis, G. S. Grubbs II, The chirped pulse, Fourier transform microwave spectrum of 1-chloromethyl-1-fluorosilacyclopentane, J. Mol. Spectrosc. 395 (2023) 111793, https://doi.org/10.1016/j.jms.2023.111793.
[4] N.T. Moon, F.E. Marshall, T.M.C. McFadden, E.J. Ocola, J. Laane, G.A. Guirgis, G. S. Grubbs II, Pure rotational spectrum and structural determination of 1,1-difluoro-1-silacyclopentane, J. Mol. Struct. 1249 (2022) 131563, https://doi.org/10.1016/j.molstruc.2021.131563.
[5] T.M.C. McFadden, F.E. Marshall, E.J. Ocola, J. Laane, G.A. Guirgis, G.S. Grubbs II, Theoretical calculations, microwave spectroscopy, and ring-puckering vibrations of 1,1-dihalosilacyclopent-2-enes, J. Phys. Chem. A 124 (2020) 8254–8262, https://doi.org/10.1021/acs.jpca.0c07250.
[6] T.M.C. McFadden, N. Moon, F.E. Marshall, A.J. Duerden, E.J. Ocola, J. Laane, G. A. Guirgis, G.S. Grubbs II, The molecular structure and curious motions in 1,1-difluorosilacyclopent-3-ene and silacyclopent-3-ene as determined by microwave

spectroscopy and quantum chemical calculations, Phys. Chem. Chem. Phys. 24 (2022) 2454–2464, https://doi.org/10.1039/d1cp04286f.
[7] L. Licaj, N. Moon, G.S. Grubbs II, G.A. Guirgis, N.A. Seifert, Broadband microwave spectroscopy of cyclopentylsilane and 1,1,1-trifluorocyclopentylsilane, J. Mol. Spectrosc. 390 (2022) 111698, https://doi.org/10.1016/j.jms.2022.111698.
[8] A. Jabri, F.E. Marshall, W.R.N. Tonks, R.E. Brenner, D.J. Gillcrist, C.J. Wurrey, I. Kleiner, G.A. Guirgis, G.S. Grubbs II, The conformational landscape, internal rotation, and structure of 1,3,5-trisilapentane using broadband rotational spectroscopy and quantum chemical calculations, J. Phys. Chem. A 124 (2020) 3825–3835, https://doi.org/10.1021/acs.jpca.0c01100.
[9] A.R. Davies, A.G. Hanna, A. Lutas, G.A. Guirgis, G.S. Grubbs II, Rotational spectrum, structure, and quadrupole coupling of cyclopropylchloromethyldifluorosilane, J. Chem. Phys. 160 (2024), https://doi.org/10.1063/5.0203016.
[10] A.H. Sharbaugh, Microwave determination of the molecular structure of chlorosilane, Phys. Rev. 74 (1948) 1870, https://doi.org/10.1103/PhysRev.74.1870.
[11] W. Zeil, W. Braun, B. Haas, H. Knehr, F. Rückert, M. Dakkouri, Mikrowellenspektrum und rotationsspektroskopische Konstanten der Methylchlorsilane: CH_3 SiH_2 Cl, CH_3 SiD_2 Cl und CD_3 SiD_2 Cl/microwave spectrum and rotational spectroscopic constants of methyl-chloro-silane: CH_3 SiH_2 Cl, CH_3 SiD_2 Cl and CD_3 SiD_2 Cl, Zeitschrift Für Naturforschung A 30 (1975) 1441–1446, https://doi.org/10.1515/zna-1975-1112.
[12] J.R. Durig, R.O. Carter, Y.S. Li, Spectra and structure of some silicon-containing compounds, J. Mol. Spectrosc. 44 (1972) 18–31, https://doi.org/10.1016/0022-2852(72)90190-7.
[13] H.-G. Kraft, B. Haas, W. Zeil, Mikrowellen-Spektrum und Struktur des Methyldichlorsilans/The microwave spectroscopy and the structures of methyl-dichloro-silane, Zeitschrift Für Naturforschung A 34 (1979) 1458–1462, https://doi.org/10.1515/zna-1979-1210.
[14] M. Mitzlaff, R. Holm, H. Hartmann, Mikrowellenspektrum Struktur Und Dipolmoment Von Trichiorsilan Und Methyltrichlorsilan, Zeitschrift Für Naturforschung A 22 (1967) 1415–1418, https://doi.org/10.1515/zna-1967-0922.
[15] W. Zeil, B. Haas, Rotationskonstante und Kernquadrupolkopplungskonstante des Trimethylehlorsilans, bestimmt aus Mikrowellenspektren/Rotational constant and nuclear quadrupole coupling constant of trimethylchlorosilane, determined by microwave spectrum, Zeitschrift Für Naturforschung A 28 (1973) 1230–1232, https://doi.org/10.1515/zna-1973-0733.
[16] R. Kewley, P.M. McKinney, A.G. Robiette, The microwave spectra and molecular structures of the silyl halides, J. Mol. Spectrosc. 34 (1970) 390–398, https://doi.org/10.1016/0022-2852(70)90022-6.
[17] H. Takeo, C. Matsumura, The microwave spectra, molecular structures, and quadrupole coupling constants of methyltrichlorosilane and trichlorosilane, Bull. Chem. Soc. Jpn. 50 (1977) 1633–1634, https://doi.org/10.1246/bcsj.50.1633.
[18] K. Endo, H. Takeo, C. Matsumura, The microwave spectrum, structure, quadrupole coupling constants, and barrier to internal rotation of methyldichlorosilane, Bull. Chem. Soc. Jpn. 50 (1977) 626–630, https://doi.org/10.1246/bcsj.50.626.
[19] I. Merke, W. Stahl, S. Kassi, D. Petitprez, G. Wlodarczak, Internal rotation, quadrupole coupling, and structure of (CH3)3SiCl studied by microwave spectroscopy and ab initio calculation, J. Mol. Spectrosc. 216 (2002) 437–446, https://doi.org/10.1006/jmsp.2002.8632.
[20] L.B. Favero, G. Maccaferri, W. Caminati, M. Grosser, M. Dakkouri, Potential energy surface of the ring puckering motion in 1-chloro-1-silacyclobutane, J. Mol. Spectrosc. 176 (1996) 321–328, https://doi.org/10.1006/jmsp.1996.0093.
[21] Y. Kawashima, The rotational spectrum of chlorodimethylsilane using Fourier transform microwave spectroscopy, J. Mol. Struct. 563–564 (2001) 227–230, https://doi.org/10.1016/S0022-2860(00)00879-6.
[22] J. Demaison, H. Šormova, H. Bürger, L. Margulès, F.L. Constantin, A. Ceausu-Velcescu, Pure rotational spectrum, ab initio anharmonic force field, and equilibrium structure of silyl chloride, J. Mol. Spectrosc. 232 (2005) 323–330, https://doi.org/10.1016/j.jms.2005.05.004.
[23] G. Cazzoli, C. Puzzarini, J. Gauss, Rotational spectrum of silyl chloride: hyperfine structure and equilibrium geometry, Mol. Phys. 110 (2012) 2359–2369, https://doi.org/10.1080/00268976.2012.680518.
[24] K.D. Hensel, W. Jager, M.C.L. Gerry, I. Merke, The Cl nuclear quadrupole coupling tensor of dichlorosilane, SiH2Cl2, J. Mol. Spectrosc. 158 (1993) 131–139, https://doi.org/10.1006/jmsp.1993.1060.
[25] R.H. Schwendeman, G.D. Jacobs, Microwave spectrum, structure, quadrupole coupling constants, and barrier to internal rotation of chloromethylsilane, J. Chem. Phys. 36 (1962) 1251–1257, https://doi.org/10.1063/1.1732722.
[26] G.A. Guirgis, D.K. Sawant, R.E. Brenner, B.S. Deodhar, N.A. Seifert, Y. Geboes, B. H. Pate, W.A. Herrebout, D.V. Hickman, J.R. Durig, Microwave, r0 structural parameters, conformational stability, and vibrational assignment of (chloromethyl) fluorosilane, J. Phys. Chem. A 119 (2015) 11532–11547, https://doi.org/10.1021/acs.jpca.5b06679.
[27] D. Barrett, J.H. Carpenter, The millimeter-wave spectrum of chlorosilane, J. Mol. Spectrosc. 107 (1984) 153–159, https://doi.org/10.1016/0022-2852(84)90274-1.
[28] M. Tanimoto, S. Saito, Y. Endo, E. Hirota, The microwave spectrum of the SiCl radical, J. Mol. Spectrosc. 103 (1984) 330–336, https://doi.org/10.1016/0022-2852(84)90060-2.
[29] J.L. Duncan, J.L. Harvie, D.C. McKean, S. Cradock, The ground state structures of disilane, methyl silane and the silyl halides, and an SiH bond length correlation with stretching frequency, J. Mol. Struct. 145 (1986) 225–242, https://doi.org/10.1016/0022-2860(86)85027-X.
[30] M. Tanimoto, H. Takeo, C. Matsumura, M. Fujitake, E. Hirota, Microwave spectroscopic detection of dichlorosilylene SiCl2 in the ground state, J. Chem. Phys. 91 (1989) 2102–2107, https://doi.org/10.1063/1.457070.
[31] R.W. Davis, M.C.L. Gerry, The microwave spectrum, structure, chlorine nuclear quadrupole coupling constants, dipole moment, and centrifugal distortion constants of dichlorosilane, J. Mol. Spectrosc. 60 (1976) 117–129, https://doi.org/10.1016/0022-2852(76)90120-X.
[32] M. Nakata, H. Takeo, C. Matsumura, Microwave spectrum of dimethyldichlorosilane, J. Mol. Spectrosc. 82 (1980) 117–126, https://doi.org/10.1016/0022-2852(80)90103-4.
[33] N. Heineking, J.-U. Grabow, I. Merke, Molecular beam Fourier transform microwave spectra of (chloromethyl)cyclopropane and (chloromethyl)oxirane, J. Mol. Struct. 612 (2002) 231–244, https://doi.org/10.1016/S0022-2860(02)00094-7.
[34] N.A. Seifert, G.A. Guirgis, B.H. Pate, The molecular structure of methyl(difluoro) silyl chloride as determined by broadband microwave spectroscopy, J. Mol. Struct. 1023 (2012) 222–226, https://doi.org/10.1016/j.molstruc.2012.04.078.
[35] A. Duerden, F.E. Marshall, N. Moon, C. Swanson, K.M. Donnell, G.S. Grubbs II, A chirped pulse Fourier transform microwave spectrometer with multi-antenna detection, J. Mol. Spectrosc. 376 (2021), https://doi.org/10.1016/j.jms.2020.111396.
[36] F.E. Marshall, D.J. Gillcrist, T.D. Persinger, S. Jaeger, C.C. Hurley, N.E. Shreve, N. Moon, G.S. Grubbs II, The CP-FTMW spectrum of bromoperfluoroacetone, J. Mol. Spectrosc. 328 (2016) 59–66, https://doi.org/10.1016/j.jms.2016.07.014.
[37] G. Sedo, F.E. Marshall, G.S. Grubbs II, Rotational spectra of the low energy conformers observed in the (1R)-(−)-myrtenol monomer, J. Mol. Spectrosc. 356 (2019) 32–36, https://doi.org/10.1016/j.jms.2018.12.005.
[38] Z. Kisiel, J. Kosarzewski, Identification of trace 2-chloropropene with a new chirped pulse microwave spectrometer, Acta Phys. Pol. A 131 (2017) 311–317, https://doi.org/10.12693/APhysPolA.131.311.
[39] Z. Kisiel, Programs for ROtational SPEctroscopy (PROSPE), http://info.ifpan.edu.pl/~kisiel/prospe.htm (accessed June 04, 2024).
[40] H.M. Pickett, The fitting and prediction of vibration-rotation spectra with spin interactions, J. Mol. Spectrosc. 148 (1991) 371–377, https://doi.org/10.1016/0022-2852(91)90393-O.
[41] Z. Kisiel, L. Pszczółkowski, I.R. Medvedev, M. Winnewisser, F.C. De Lucia, E. Herbst, Rotational spectrum of trans-trans diethyl ether in the ground and three excited vibrational states, J. Mol. Spectrosc. 233 (2005) 231–243, https://doi.org/10.1016/j.jms.2005.07.006.
[42] M. J. Frisch, G.W. Trucks, H.B. Schlegel, G.E. Scuseria, M.A. Robb, J.R. Cheeseman, G. Scalmani, V. Barone, G.A. Petersson, H. Nakatsuji, X. Li, M. Caricato, A.V. Marenich, J. Bloino, B.G. Janesko, R. Gomperts, B. Mennucci, H.P. Hratchian, J.V. Ortiz, A.F. Izmaylov, J.L. Sonnenberg, D. Williams-Young, F. Ding, F. Lipparini, F. Egidi, J. Goings, B. Peng, A. Petrone, T. Henderson, D. Ranasinghe, V.G. Zakrzewski, J. Gao, N. Rega, G. Zheng, W. Liang, M. Hada, M. Ehara, K. Toyota, R. Fukuda, J. Hasegawa, M. Ishida, T. Nakajima, Y. Honda, O. Kitao, H. Nakai, T. Vreven, K. Throssell, J.A. Montgomery Jr., J.E. Peralta, F. Ogliaro, M.J. Bearpark, J.J. Heyd, E.N. Brothers, K.N. Kudin, V.N. Staroverov, T.A. Keith, R. Kobayashi, J. Normand, K. Raghavachari, A.P. Rendell, J.C. Burant, S.S. Iyengar, J. Tomasi, M. Cossi, J.M. Millam, M. Klene, C. Adamo, R. Cammi, J.W. Ochterski, R.L. Martin, K. Morokuma, O. Farkas, J.B. Foresman, D.J. Fox, Gaussian 16, Revision C.01, 2016.
[43] E.D. Glendening, A.E. Reed, J.E. Carpenter, F. Weinhold, NBO Version 3.1, (n.d.).
[44] U. Spoerel, H. Dreizler, W. Stahl, Notizen: on the sign of the off-diagonal elements of the nuclear quadrupole coupling tensor, Zeitschrift Für Naturforschung A 49 (1994) 645–646, https://doi.org/10.1515/zna-1994-4-522.
[45] A.C. Legon, J.C. Thorn, Equilibrium nuclear quadrupole coupling constants from the rotational spectrum of BrCl: a source of the electric quadrupole moment ratios Q (79 Br)/Q (81 Br) and Q (35 Cl)/Q (37 Cl), Chem. Phys. Lett. 215 (1993) 554–560, https://doi.org/10.1016/0009-2614(93)89354-K.
[46] C.H. Townes, A.L. Schawlow, Microwave Spectroscopy, Dover Publications, Inc., New York, 2012.
[47] C.H. Townes, B.P. Dailey, Determination of electronic structure of molecules from nuclear quadrupole effects, J. Chem. Phys. 17 (1949) 782–796, https://doi.org/10.1063/1.1747400.
[48] S.E. Novick, Extended Townes-Dailey analysis of the nuclear quadrupole coupling tensor, J. Mol. Spectrosc. 267 (2011) 13–18, https://doi.org/10.1016/j.jms.2011.01.004.
[49] W. Gordy, R.L. Cook, Microwave Molecular Spectra, third edition, John Wiley & Sons, New York, 1984.
[50] J. Kraitchman, Determination of molecular structure from microwave spectroscopic data, Am. J. Phys. 21 (1953) 17–24, https://doi.org/10.1119/1.1933338.
[51] C.C. Costain, Determination of molecular structures from ground state rotational constants, J. Chem. Phys. 29 (1958) 864–874, https://doi.org/10.1063/1.1744602.
[52] L. Pierce, Note on the use of ground-state rotational constants in the determination of molecular structures, J. Mol. Spectrosc. 3 (1959) 575–580, https://doi.org/10.1016/0022-2852(59)90049-9.
[53] L.C. Krisher, L. Pierce, Second differences of moments of inertia in structural calculations: application to methyl-fluorosilane molecules, J. Chem. Phys. 32 (1960) 1619–1625, https://doi.org/10.1063/1.1730993.
[54] Y. Morino, Y. Murata, Mean-square amplitudes and force constants of tetrahedral molecules. II. Silicon tetrachloride, Bull. Chem. Soc. Jpn. 38 (1965) 104–113, https://doi.org/10.1246/bcsj.38.104.